


LETTER

Open Access



Hybrid optical parametrically-oscillating emitter at 1930 nm for volumetric photoacoustic imaging of water content

Jiawei Shi^{1†}, Mingsheng Li^{1†}, Huajun Tang¹, Jiqiang Kang^{1,3}, Najia Sharmin¹, Amir Rosenthal² and Kenneth K. Y. Wong^{1,3*} 

Abstract

Water plays a vital role in biological metabolism and it would be essential to trace the water content non-invasively, such as leveraging the vibrational absorption peak of the O–H bond. However, due to the lack of an efficient laser source, it was challenging to image the water content in the deep tissue with micron-level spatial resolution. To address this problem, we develop a high-power hybrid optical parametrically-oscillating emitter (HOPE) at 1930 nm, at which the vibrational absorption peak of the O–H bond locates. The maximum pulse energy is over 1.74 μJ with a pulse repetition rate of 50 kHz and a pulse width of 15 ns. We employ this laser source in the optical-resolution photoacoustic microscopy (OR-PAM) system to image the water content in the phantom and the biological tissue in vitro. Our 1930-nm OR-PAM could map the water content in the complex tissue environment at high spatial resolution, deep penetration depth, improved sensitivity, and suppressed artifact signal of the lipid.

Keywords: Fiber optical parametric oscillator, Thulium-doped fiber laser, Photoacoustic microscopy

Vibrational photoacoustic imaging (PAI) at the near-infrared region provides a powerful label-free imaging tool for sensing the chemical bonds in the deep tissue [1–6]. Via the molecular overtone transitions and combinational band absorptions, the vibration-based PA signal could be generated for imaging the specific chemical bond-rich tissues. It has been developed into multiple branches, such as the high-speed intravascular vibrational photoacoustic catheter for imaging lipid-laden plaques [7, 8], vibration-based photoacoustic tomography for mapping the margin of the breast cancer [9] and the femoral nerves discriminated from the femoral artery [10].

Water is a vital component closely relevant to biological metabolism. Mapping the water content would be beneficial to analyze the biological and pathological properties of the cells, tissues, and organs. For the PAI technique, to visualize the water content in the deep tissue with high spatial resolution and good SNR, the laser source should have high laser pulse energy, fast pulse repetition rate, and accurate wavelength tunability at which water has relatively strong absorption [11–14]. However, before that, only a few works have been reported to use PAI to image the water distribution due to the lack of suitable laser sources. Xu et al. employed a tunable OPO laser operating at around 1000 nm along with a photoacoustic computed tomography system to image the water content in the phantom and mice's brain [15, 16]. It indicated that PAI could have the potential to image water distribution in the deep tissue.

Owing to the relatively low absorption of water at around 1000 nm, it usually required milli-joule level pulse energy, which may induce photodamage in the tissue. In

*Correspondence: kywong@eee.hku.hk

[†]Jiawei Shi and Mingsheng Li are contributed equally to this work

¹ Department of Electrical and Electronic Engineering, The University of Hong Kong, Pokfulam Road, Hong Kong, China

Full list of author information is available at the end of the article

addition, OPO laser with the high cost and low pulse repetition rate makes it not a perfect choice for high-speed PAI for clinical applications. At the SWIR region (900–2000 nm), the water has significantly stronger absorption, involving multiple absorption peaks located at 975 nm, 1160 nm, 1450 nm, and 1930 nm [17]. Among them, the absorption coefficient of water at 1930 nm is the strongest, reaching 117.6 cm^{-1} . Moreover, the absorption of lipid at 1930 nm is 2.11 cm^{-1} , which is close to two orders of magnitude smaller than the water’s absorption. The initial PA amplitude could be expressed as, $p_0 = k\Gamma\mu_a F$, where k is a constant related to the imaging system, Γ is the Grüneisen parameter of the chromophore, μ_a is the absorption coefficient, and F is the local laser fluence. For the same laser and pulse energy, the PA signals generated from different chromophores should be proportional to $\Gamma\mu_a$. Therefore, the PA contrast of water versus lipid at 1930 nm could be expressed as $P_{\text{water}}/P_{\text{lipid}} = (\Gamma\mu_a)_{\text{water}}/(\Gamma\mu_a)_{\text{lipid}}$. Because the Grüneisen parameter of lipid and water are 0.7–0.9 and 0.12 at 22 °C, respectively, the PA

contrast of water versus lipid at 1930 nm is 7.7–10. From the analysis above, vibration PAI at 1930 nm could image the water content with higher sensitivity and finer signal-to-noise ratio (SNR). Meanwhile, the artifact signal arising from the lipid in the complex environment could be suppressed at 1930 nm. These features make 1930-nm pulsed laser a suitable choice to map the water content using the PAI technique.

Recently, the fiber lasers at the SWIR region have drawn growing interests in biomedical imaging and bio-sensing [18–20]. Thulium-doped fiber amplifier (TDFA) pumped by an Er/Yb-doped fiber laser provides the gain over 30 dB in the wavelength range over 100 nm around 1900 nm. Empowered by the significant gain offered by the Tm³⁺ ion, TDFL can be able to emit high-power laser pulses with a high repetition rate for generating PA signal efficiently [21–23]. In our previous works, a tunable thulium-assisted fiber optical parametric oscillator (TAOPO) from 1700 to 2100 nm has been developed with a pulse width of 2 ns at 3.2 MHz [23]. Hindered by

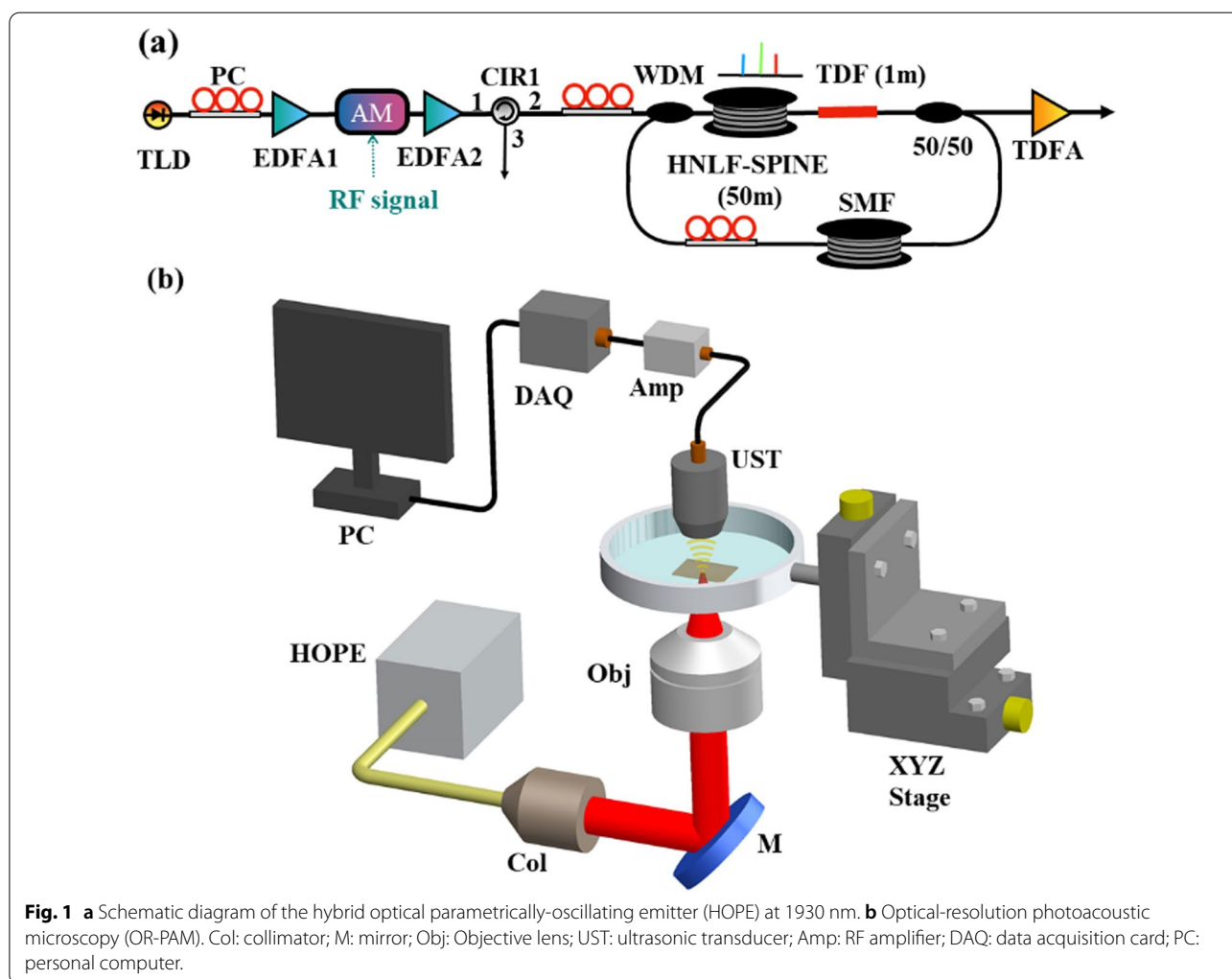
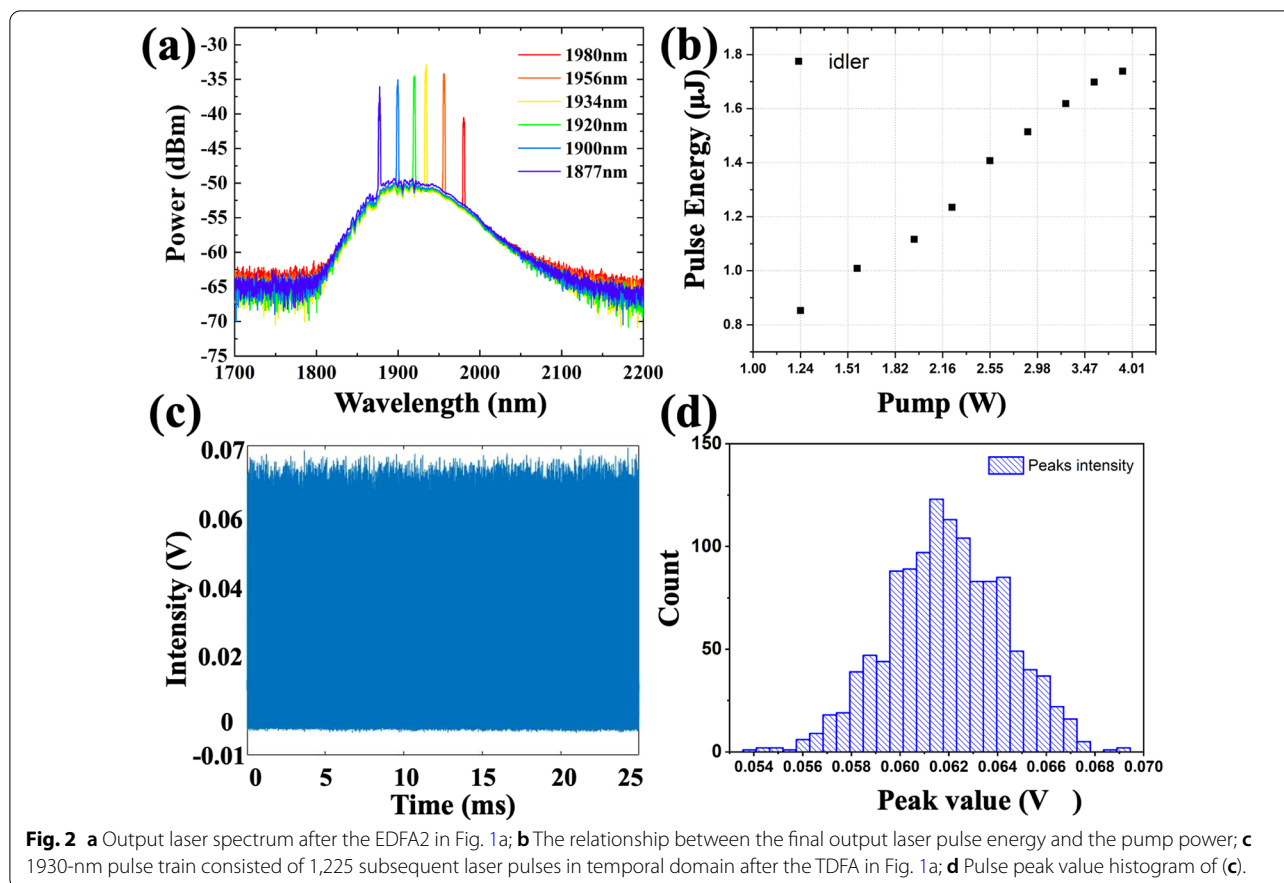


Fig. 1 **a** Schematic diagram of the hybrid optical parametrically-oscillating emitter (HOPE) at 1930 nm. **b** Optical-resolution photoacoustic microscopy (OR-PAM). Col: collimator; M: mirror; Obj: Objective lens; UST: ultrasonic transducer; Amp: RF amplifier; DAQ: data acquisition card; PC: personal computer.



the high repetition rate and insufficient gain inside the fiber cavity, the maximum pulse energy is only ~ 162 nJ, inadequate for biological tissue PAI at the SWIR region.

In this letter, we report a type of high-power all-fiber hybrid optical parametrically-oscillating emitter at 1930 nm, and the system is abbreviated as HOPE here. HOPE consists of a fiber optical parametric oscillator and a segment of TDF, and it generates 15-ns laser pulses at 1930 nm with 1-nm bandwidth and single pulse energy over $1.74 \mu\text{J}$ at the pulse repetition rate of 50 kHz. To verify the system performance, the volumetric water content imaging experiment using a phantom and an *in-vitro* fresh biological tissue was conducted by launching the output pulses of the HOPE system to a home-built optical-resolution photoacoustic microscopy (OR-PAM) system. Moreover, the performance of OR-PAM in imaging the water and lipid content of the adipose tissue are explored and compared by using 1930-nm and 1750-nm pulses.

Figure 1a depicts the schematic diagram of the 1930-nm HOPE system. The pump for the parametric conversion process was seeded by a tunable laser source (TLD). The output of the TLD was firstly amplified to 10 mW through a low-power erbium-doped fiber amplifier

(EDFA1) and then launched into a Mach–Zehnder amplitude modulator (AM) to generate rectangular pulses. The AM was driven by a radio frequency (RF) signal with a 15 ns pulse width at a 50 kHz repetition rate which corresponds to a 0.075% duty ratio. Followed by that, a tunable bandpass filter with 1-nm spectral bandwidth filtered the undesired amplified spontaneous emission (ASE), and a high power EDFA (EDFA2) was cascaded to boost the average power of the laser pulse train to 2-W. The peak power of the pulses after the EDFA2 was 2.67 kW. After passing through a fiber circulator (CIR1), the high-energy 1560-nm pulsed laser was delivered into the cavity via a 1950/1550 nm fiber wavelength-division-multiplexing coupler (WDM). The parametric conversion occurred when the pump pulses passed through a spool of 50-m highly nonlinear fiber (HNLF-SPINE, OFS), which performed as the parametric gain medium in the cavity. In principle, distinct and narrowband gain regions can be obtained when the pump was operating at the normal dispersion regime [29]. Via carefully tuning the polarization state of the laser by the polarization controller (PC), the four-wave mixing process could convert the pump energy to a narrowband idler at the wavelength from 1800 to 2000 nm with pump wavelength tuned from 1541

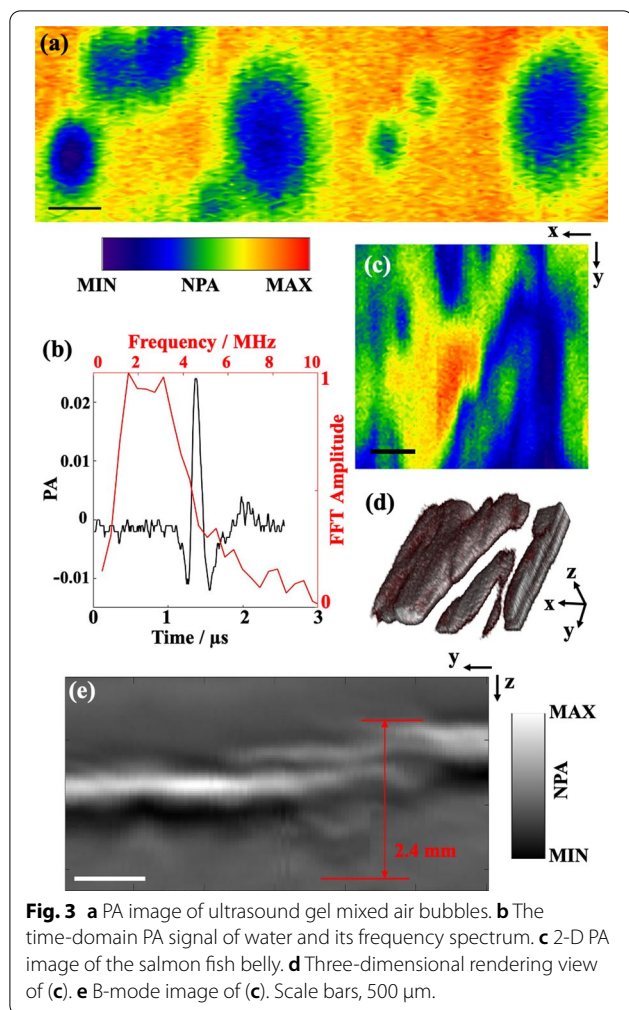


Fig. 3 **a** PA image of ultrasound gel mixed air bubbles. **b** The time-domain PA signal of water and its frequency spectrum. **c** 2-D PA image of the salmon fish belly. **d** Three-dimensional rendering view of (c). **e** B-mode image of (c). Scale bars, 500 μm .

to 1563 nm. Subsequently, the idler was amplified via a 1-m TDF (OFS-TmDF200), in which the residual pump at the 1550-nm band was further depleted for boosting the idler power to enhance the cavity gain. In this process, the idler provided a narrowband seed signal to TDF, which made the amplified output energy more concentrated in the wavelength of interest 1930 nm, which results in the output laser pulse with an improved SNR. After the TDF, the idler power was measured over 10 dB higher than the residual pump in the optical spectrum analyzer (OSA, Yokogawa, AQ6375). A 50/50 fiber coupler was connected to the TDF, of which one stream outputted the laser for external amplification and another stream guided the idler back to the input port of the cavity via the 1950-nm port of WDM. A spool of 200 m single-mode fiber (SMF) was utilized to increase the cavity length, and the total length of the cavity is around 267 m, corresponding to the 750 kHz fundamental cavity repetition rate. It should be noted that the modulation repetition rate of the AM was set as 50 kHz rather

than 750 kHz for higher pulse energy generation. The output 1930-nm pulses were further boosted by another TDEFA outside the cavity with an extra 1.5-W pumping at 1650 nm. The final output average power of the 1930-nm pulses was 53.4 mW, and the corresponding single pulse energy is 1.07 μJ . The output spectra were captured by the OSA, as shown in Fig. 2a. Nearly all of the residual pump power from OPO and TDEFA was depleted out, and only amplified idler can be observed in the OSA. When the pump wavelength was tuned from 1551 to 1559 nm, the idler wavelength could be adjusted from 1877 to 1980 nm. It is worthy to note that the idler at around 1934 nm in Fig. 2a experienced the maximum gain at TDE. The maximum gain was realized by adjusting the TDF length via the cutting-back method to 7.86 m, where the gain spectrum peak was moved to the desired wavelength, i.e., 1930 nm. The output power and pulse stability at this wavelength were further examined. Figure 2b shows that the idler pulse energy increased linearly with an increased pump power from 1 to 4 W. The maximum pulse energy is 1.74 μJ . The temporal pulse train of the output was measured with a real-time oscilloscope, as shown in Fig. 2c, and its pulse intensity histogram was shown in Fig. 2d. The standard deviation to the mean ratio (std/mean) was calculated to be 3.86% over 1225 subsequent laser pulses. The 1930-nm pulses were delivered via a 0.5-m SMF to a transmission-mode OR-PAM system (see Additional file 1).

The OR-PAM system in Fig. 1b is similar to the one in our previous works [21]. The 1930-nm laser beam was focused by an objective lens (0.1 NA, PlanN 4x, Olympus), transmitted through an optical window (UDP10, Infrasil), which provided transmission over 95% at around 1930 nm, and then illuminated the sample to excite PA signals. The sample was placed beneath the water with a thin polyethylene membrane for isolation from the water. The water at the sample surface and the water in the tank performed as the acoustic coupling agent. The whole water tank with the sample was mounted on an X–Y–Z translational stage to conduct raster-scanning. An ultrasonic transducer (V316, Olympus, 10 MHz) collected the PA wave at the same spot of light excitation and converted it to electrical signals. The electrical signals were successively amplified by two cascaded RF low-noise amplifiers (ZFL-500LN+, Mini-Circuits, 28 dB), and then filtered by a low-pass filter (BLP-10.7+, Mini-Circuits, DC-11 MHz) before being digitalized by an oscilloscope (SDA8Zi-B, Teledyne LeCroy). The UT has the center frequency at 10 MHz. Therefore, the sampling rate of the oscilloscope was set to 100 MHz. And sampling length was selected to 500, which corresponds to a 5- μs time window. Considering the sound speed in tissue (1.56 mm/ μs), the traveling distance of the PA signal in

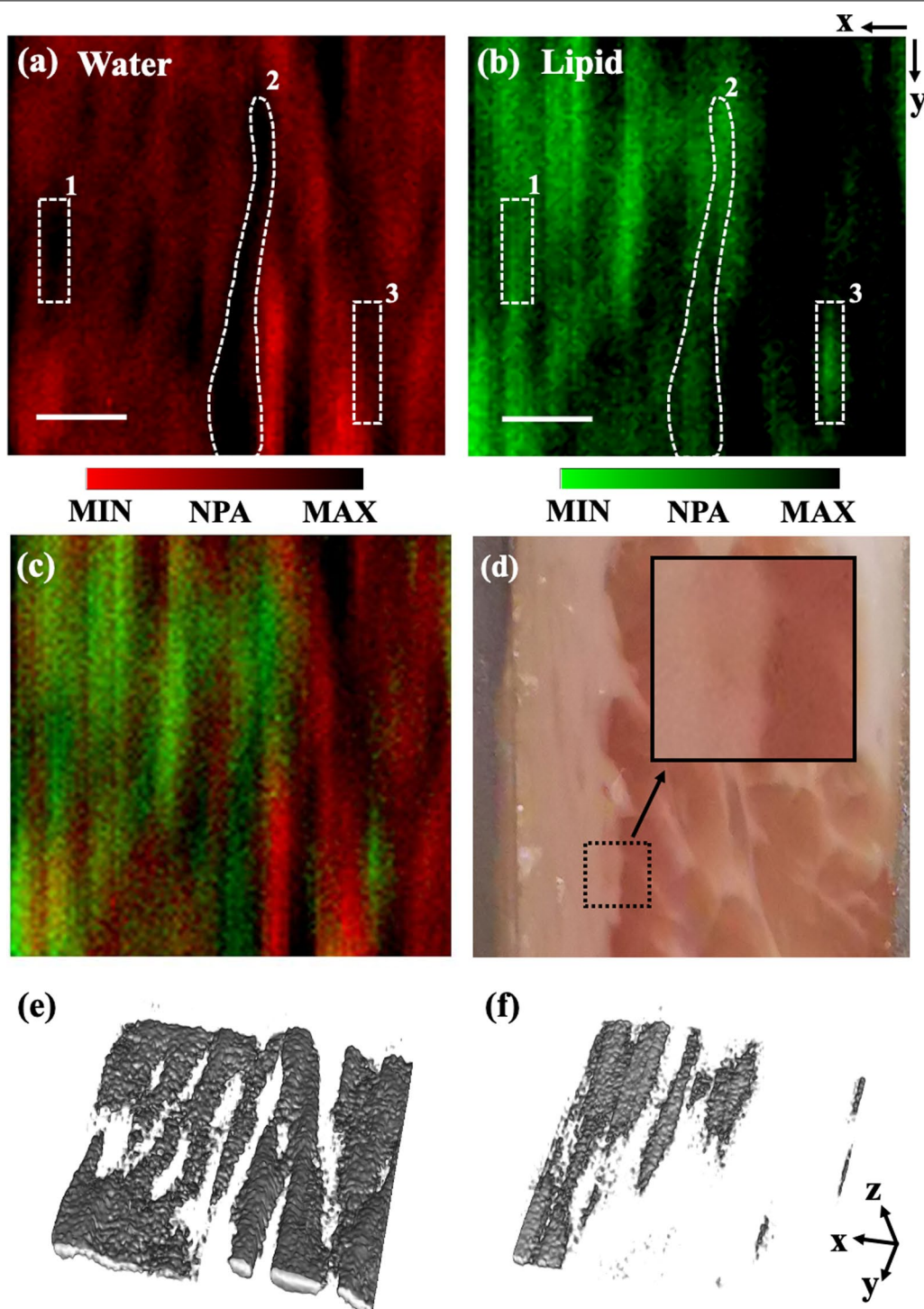


Fig. 4 PA image of (a) water acquired by 1930-nm OR-PAM and (b) lipid acquired by 1750-nm OR-PAM; (c) Overlaid PA image of (a) and (b). (d) Photography of the adipose tissue. (e–f) Three-dimensional rendering view of (a, b). Scale bars, 500 μm

this time window is calculated to 7.8 mm. It means in this time window, it is sufficient to capture all PA signals in the depth of field (~ 0.1 mm). The lateral resolution was measured as 21.2 μm (see Fig. S1 in Additional File 1).

In the phantom study, we employed our 1930-nm OR-PAM to image the ultrasound gel mixed with air bubbles, as shown in Fig. 3a. The air bubbles inside the gel

could perform as the negative-contrast agent. Here, the pulse energy of the 1930 nm laser was kept at 300 nJ, and the step size is 20 μm . The PA signal was acquired at the sampling rate of 100 MHz with averaging by four times at each pixel. Single PA signal length is 500 points, and the corresponding time window is 5 μs . We extracted one A-line after averaging, computed its SNR, and performed the frequency analysis. As shown in Fig. 3b, the A-line's SNR could reach 19 dB and its frequency mainly ranged from 1 to 4 MHz. We utilized our 1930-nm OR-PAM system to image the salmon fish belly (Fig. 3c) and showed its 3-D rendering view image (Fig. 3d). The pulse energy was adjusted to 1 μJ . The step size and averaging time kept 20 μm and 4 times. From that, the muscle texture of the salmon fish tissue could be visualized with high contrast to the adipose region. From its B-mode image in Fig. 3e, we found that our 1930-nm OR-PAM had improved penetration depth up to 2.4 mm owing to the less photon scattering in the tissue compared with the OR-PAM operating with the visible and shorter wavelength near-infrared lasers [24]. The improved penetration ability could facilitate the 1930-nm OR-PAM for quantitative imaging of water content in the deep tissue.

Finally, to demonstrate that 1930-nm OR-PAM could image the water with suppressed artifact signals from the lipid, we utilized the previously developed 1750-nm OR-PAM along with the 1930-nm OR-PAM system to image the lipid and water in the adipose tissue, then overlaid both PA images, as shown in Fig. 4a–c. The pulse energy at 1750 nm and 1930 nm were set to 5 μJ and 1 μJ respectively. The step size and averaging time kept same as the above experiments. We used the white dash line to highlighted three same regions in both PA images of water and lipid, in which the lipid PA signals were strong while the water PA signal is negligibly weak. It approved that our 1930-nm OR-PAM could visualize the water distribution in the complex tissue environment and suppressed the artifact signal arising from the lipid, which was rich in many biological tissues. Figure 4e, f were the 3-D rendering view of Fig. 4a, b and showed a coincident muscle texture of the adipose tissue.

In other related works, coherent Raman scattering (CRS) microscopy has been developed successfully to map the water in the tissue with micron-level spatial resolution, high signal-to-noise ratio (SNR), and the fine signal-to-background ratio [25]. Nevertheless, CRS microscopy utilizes all-optical excitation and detection, resulting in the limited penetration depth due to the strong scattering of light inside the biological tissue. In addition, CRS microscopy requires the pico- or

femtosecond pulse-width laser, whose expensive costs make this technique less accessible and commercialized. Other label-free optical imaging techniques at short-wave infrared (SWIR) wavelength region for water imaging require expensive InGaAs and germanium detectors, commercially available in recent years [26–29]. Owing to the strong absorption of water at 1930 nm ($\mu_a = 117.6\text{cm}^{-1}$), using 15-ns pulse with only sub-mJ pulse energy, the 1930-nm OR-PAM offers absorption-based optical contrast, acoustic penetration ability, and an imaging sensitivity eight orders of magnitude larger than the Raman imaging technique [14]. It could image the water with good SNR \sim 19 dB and penetrate up to 2.4 mm in the tissue, which is much deeper than the Raman imaging technique as well as the visible and near-infrared band OR-PAM due to the less photon scattering in the tissue. More importantly, the water versus lipid PA contrast ratio at 1930 nm is 7.7–10, enabling the 1930-nm OR-PAM to image water distribution with suppressed artifact signal generating from the lipid, which was one of the most common components in the biological tissues. Moreover, 1930-nm OR-PAM could also operate in the epi-mode for in vivo application. To mitigate the laser attenuation, heavy water or heavy water-based ultrasound gel could be used as the ultrasound coupling medium [30].

In conclusion, we reported a novel high-power HOPE at 1930 nm. The 1930-nm pulse energy was over 1.74 μJ with a pulse repetition rate of 50 kHz and pulse width of 15 ns. With the HOPE system, we developed a vibrational optical-resolution photoacoustic microscopy system to detect the O–H bond in the water, aqueous sample, and biological tissue in vitro. It could image the water distribution in the deep tissue with micron-level spatial resolution, fine SNR, improved penetration depth, and suppressed artifact signal. These excellent advantages could help this technique open a broad avenue for biological research and disease diagnosis.

Abbreviations

HOPE: Hybrid optical parametrically-oscillating emitter; PAI: Photoacoustic imaging; PA: Photoacoustic; OR-PAM: Optical-resolution photoacoustic microscopy; CRS: Coherent Raman scattering; SNR: Signal-to-noise ratio; SWIR: Short-wave infrared; OPO: Optical parametric oscillator; RF: Radio frequency; TLD: Tunable laser diode; AM: Amplitude modulator; PC: Polarization controller; EDFA: Erbium-doped fiber amplifier; TDF: Thulium-doped fiber; TDFA: Thulium-doped fiber laser; SMF: Single-mode fiber; CIR: Circulator; WDM: Wavelength-division multiplexing coupler; HNLF-SPINE: Highly nonlinear fiber with stable phase-matching for improved nonlinear efficiency; Col: Collimator; M: Mirror; Obj: Objective lens; UST: Ultrasonic transducer; Amp: RF amplifier; DAQ: Data acquisition card; PC: Personal computer.

Supplementary Information

The online version contains supplementary material available at <https://doi.org/10.1186/s43593-022-00014-2>.

Additional file 1: Figure S1. Line scanning of carbon fiber (10 μm) with a step size of 2 μm . **Figure S2. a** PA image of water mixed with silicone oil droplets; **b** Three-dimensional rendering view of **(a)**. **Figure S3. a** PA image of beef muscular tissue; **b** Three-dimensional rendering view of **(a)**. **Table S1.** Specification of three fiber lasers. **Table S2.** Specification of all imaging experiments.

Authors' contributions

KKYW and AR proposed the technique and designed the experiment. JS, ML, and HT performed the experiment. JS, and ML wrote the manuscript. All authors contributed to the analysis of the data and discussion and revision of the manuscript. All authors read and approved the final manuscript.

Funding

This project is funded by Research Grants Council of the Hong Kong Special Administrative Region, China (HKU 17200219, HKU 17209018, E-HKU701/17, CityU T42-103/16-N, and HKU C7047-16G) and Natural Science Foundation of China (N_HKU712/16).

Availability of data and materials

The datasets used and/or analysed during the current study are available from the corresponding author on reasonable request.

Declarations

Competing interests

The authors declare no competing financial interests.

Author details

¹Department of Electrical and Electronic Engineering, The University of Hong Kong, Pokfulam Road, Hong Kong, China. ²Department of Electrical Engineering, Technion–Israel Institute of Technology, Technion City, 32000 Haifa, Israel. ³Advanced Biomedical Instrumentation Centre, Hong Kong Science Park, Shatin, New Territories, Hong Kong, China.

Received: 10 June 2021 Revised: 26 September 2021 Accepted: 23 March 2022

Published online: 26 April 2022

References

- J. Hui, Q. Yu, T. Ma, P. Wang, Y. Cao, R.S. Bruning, Y. Qu, Z. Chen, Q. Zhou, M. Sturek, J.-X. Cheng, W. Chen, High-speed intravascular photoacoustic imaging at 17 μm with a KTP-based OPO. *Biomed. Opt. Express* **6**, 4557 (2015)
- P. Wang, H.-W. Wang, M. Sturek, J.-X. Cheng, Bond-selective imaging of deep tissue through the optical window between 1600 and 1850 nm. *J. Biophotonics* **5**, 25–32 (2012)
- H.-W. Wang, N. Chai, P. Wang, S. Hu, W. Dou, D. Umulis, L.V. Wang, M. Sturek, R. Lucht, J.-X. Cheng, Label-free bond-selective imaging by listening to vibrationally excited molecules. *Phys. Rev. Lett.* **106**, 238106 (2011)
- Y. Li, X. Gong, C. Liu, R. Lin, W. Hau, X. Bai, L. Song, High-speed intravascular spectroscopic photoacoustic imaging at 1000 A-lines per second with a 0.9-mm diameter catheter. *J. Biomed. Opt.* **20**, 1 (2015)
- P. Wang, P. Wang, H.-W. Wang, J.-X. Cheng, Mapping lipid and collagen by multispectral photoacoustic imaging of chemical bond vibration. *J. Biomed. Opt.* **17**, 0960101 (2012)
- P. Wang, J.R. Rajian, J.-X. Cheng, Spectroscopic imaging of deep tissue through photoacoustic detection of molecular vibration. *J. Phys. Chem. Lett.* **4**, 2177–2185 (2013)
- P. Wang, T. Ma, M.N. Slipchenko, S. Liang, J. Hui, K.K. Shung, S. Roy, M. Sturek, Q. Zhou, Z. Chen, J.-X. Cheng, High-speed intravascular photoacoustic imaging of lipid-laden atherosclerotic plaque enabled by a 2-kHz barium nitrite raman laser. *Sci Rep* **4**, 1–7 (2014)
- J.R. Rajian, R. Li, P. Wang, J.-X. Cheng, Vibrational photoacoustic tomography: chemical imaging beyond the Ballistic Regime. *J. Phys. Chem. Lett.* **4**, 3211–3215 (2013)
- R. Li, P. Wang, L. Lan, F.P. Lloyd, C.J. Goergen, S. Chen, J.-X. Cheng, Assessing breast tumor margin by multispectral photoacoustic tomography. *Biomed. Opt. Express* **6**, 1273 (2015)
- R. Li, E. Phillips, P. Wang, C.J. Goergen, J.-X. Cheng, Label-free in vivo imaging of peripheral nerve by multispectral photoacoustic tomography. *J. Biophotonics* **9**, 124–128 (2016)
- M. Diem, A. Mazur, K. Lenau, J. Schubert, B. Bird, M. Miljković, C. Krafft, J. Popp, Molecular pathology via IR and Raman spectral imaging. *J. Biophotonics* **6**, 855–886 (2013)
- D. Zhang, C. Li, C. Zhang, M.N. Slipchenko, G. Eakins, J.-X. Cheng, Depth-resolved mid-infrared photothermal imaging of living cells and organisms with submicrometer spatial resolution. *Sci. Adv.* **2**, e1600521 (2016)
- C. Zhang, J.-X. Cheng, Perspective: coherent raman scattering microscopy, the future is bright. *APL Photonics* **3**, 090901 (2018)
- M.A. Pleitez, A.A. Khan, A. Soldà, A. Chmyrov, J. Reber, F. Gasparin, M.R. Seeger, B. Schätz, S. Herzig, M. Scheideler, V. Ntziachristos, Label-free metabolic imaging by mid-infrared optoacoustic microscopy in living cells. *Nat. Biotechnol.* **38**, 293–296 (2020)
- Z. Xu, Q. Zhu, L.V. Wang, In vivo photoacoustic tomography of mouse cerebral edema induced by cold injury. *J. Biomed. Optics* **16**, 066020 (2011)
- Z. Xu, C. Li, L.V. Wang, Photoacoustic tomography of water in phantoms and tissue. *J. Biomed. Optics* **15**, 036019 (2010)
- J. Tian, W.D. Philpot, Relationship between surface soil water content, evaporation rate, and water absorption band depths in SWIR reflectance spectra. *Remote Sens. Environ.* **169**, 280–289 (2015)
- M. Janeczek, J. Świdorski, A. Czerski, B. Żywicka, J. Bujok, M. Szymonowicz, E. Bilewicz, M. Dobrzyński, M. Korczyński, A. Chrószcz, Z. Rybak, Preliminary evaluation of thulium doped fiber laser in pig model of liver surgery. *Biomed. Res. Int.* **2018**, 1–7 (2018)
- S. Tan, L. Yang, X. Wei, C. Li, N. Chen, K.K. Tsia, K.K.Y. Wong, High-speed wavelength-swept source at 2.0 μm and its application in imaging through a scattering medium. *Opt. Lett.* **42**, 1540 (2017)
- D.C. Kirsch, S. Chen, R. Sidharthan, Y. Chen, S. Yoo, M. Chernysheva, Short-wave IR ultrafast fiber laser systems: current challenges and prospective applications. *J. Appl. Phys.* **128**, 180906 (2020)
- C. Li, J. Shi, X. Wang, B. Wang, X. Gong, L. Song, K.K.Y. Wong, High-energy all-fiber gain-switched thulium-doped fiber laser for volumetric photoacoustic imaging of lipids. *Photonics Res.* **8**, 160 (2020)
- Z. Li, S.U. Alam, Y. Jung, A.M. Heidt, D.J. Richardson, All-fiber, ultra-wide-band tunable laser at 2 μm . *Opt. Lett.* **38**, 4739 (2013)
- C. Li, N. Chen, X. Wei, J. Kang, B. Li, S. Tan, L. Song, K.K.Y. Wong, High-power widely tunable all-fiber thulium-assisted optical parametric oscillator at SWIR band. *Opt. Lett.* **41**, 5258 (2016)
- S.L. Jacques, Optical properties of biological tissues: a review. *Phys. Med. Biol.* **58**, R37 (2013)
- C. Yang, Y. Bi, E. Cai, Y. Chen, S. Huang, Z. Zhang, P. Wang, Pulse-sheet chemical tomography by counter-propagating stimulated Raman scattering. *Optica* **8**, 396 (2021)
- L. L. Randeberg and J. Hernandez-Palacios, Hyperspectral imaging of bruises in the SWIR spectral region. *Photonic Ther. Diagn. VIII.* **8207** (2012). <https://doi.org/10.1117/12.909137>
- T. Bruns, T.S. Bischof, D.K. Harris, D. Franke, Y. Shi, L. Riedemann, A. Bartelt, F.B. Jaworski, J.A. Carr, C.J. Rowlands, M.W.B. Wilson, O. Chen, H. Wei, G.W. Hwang, D.M. Montana, I. Coropceanu, O.B. Achorn, J. Kloepper, J. Heeren, P.T.C. So, D. Fukumura, K.F. Jensen, R.K. Jain, M.G. Bawendi, Next-generation in vivo optical imaging with short-wave infrared quantum dots. *Nat. Biomed. Eng.* **1**, 0056 (2017)
- H. Akbari, Y. Kosugi, K. Kojima, N. Tanaka, Detection and analysis of the intestinal ischemia using visible and invisible hyperspectral imaging. *IEEE Trans. Biomed. Eng.* **57**, 2011–2017 (2010)
- Y. Zhao, A. Pilvar, A. Tank, H. Peterson, J. Jiang, J.C. Aster, J.P. Dumas, M.C. Pierce, D. Roblyer, Shortwave-infrared meso-patterned imaging enables label-free mapping of tissue water and lipid content. *Nat. Commun.* **11**, 1–11 (2020)
- M. Li, J. Shi, C.C.Y. Yiu, C. Li, K.K.Y. Wong, L. Wang, Near-infrared double-illumination optical-resolution photoacoustic microscopy. *J. Biophotonics* **14**, e202000392 (2020)